Original Article
Cite This: Colloid & Nanoscience Journal 2(2) (2024) 277-287.
CNJ.araku.ac.ir

Enhancing methyl orange photodegradation over a reusable Ag-TiO_2/SBA-15 nanocomposite

Alireza Yadegari[1], Mahmoud Salimi[*1]

Received:2024-10-16
Revised: 2024-10-27
Accepted: 2024-10-30
DOI: **10.61186/CNJ.2.2.277**

[1]Department of Chemical Engineering, Arak Branch, Islamic Azad University, Arak, Iran

Abstract

Currently, wastewater treatment is seen as an industrial opportunity to rejuvenate fresh water resources. It is highly needed in water stressed countries. This work presents a one-step microwave -assisted hydrothermal method for making Ag-TiO_2/SBA-15 nanophotocatalysts. XRD, N_2 adsorption-desorption isotherms-desorption isotherms, AFM, UV-Vis, and UV-DRS analysis carried out to characterize the obtained photocatalyst sample. With high Ag loading on the surface of TiO_2 nanoparticles, agglomeration of silver nanoparticles and also clogging occurs in the SBA-15 pores and confirmed by AFM analysis. The optical bandgap energies obtained by DRS analysis was significantly blue-shifted, which is the quantization effects improving photocatalytic activities under visible light illumination due to the presence of silver nanoparticles that act as photosensitizer and reduce the recombination of the formed charge carriers (e and hole). Photocatalytic performances of Ag-TiO_2/SBA-15 nanophotocatalyst were evaluated by methyl orang (MO) dye photodegradation at different Ag/TiO_2 ratios. In MO destruction experiments, the highest photocatalytic efficiency was obtained in the Ag/TiO_2-SBA-15 (Ag:TiO_2=1.0) photocatalyst at 76.0%, and all efficiencies over the synthesized nanophotocatalysts are higher than commercial bulk TiO_2 nanophotocatalyst activity due to the low UV part of the applied visible light halogen lamp and also Ag/TiO_2 nanophotocatalyst that maybe due to the poor dispersion of active phases. The highest photocatalytic efficiency was obtained in the Ag-TiO_2/SBA-15 (1.0) at pH=4. The photocatalyst can be reused six times without losing its effectiveness. This shows that the photocatalyst is stable and can be used repeatedly.

Keywords: Wastewater treatment, Photocatalysis, Methyl orange dye, Ag-TiO_2/SBA-15,

1. Introduction

Wastewater is generated by many dyes producing and dye consuming industries in their process activities, especially in the textile industry. This wastewater becomes toxic and harmful to life and the environment if not properly treated before it is released into the environment. In recent decades, dye effluent has become a growing water pollution problem [1]. It is one of the most difficult effluents to treat. There are a number of methods that can be used for the removal of color from industrial wastewater containing dyes [2]. However, many treatment methods may not be effective on their own and may need to be combined with other treatment methods to achieve maximum color removal because of the variety of dyes available and the fact that industrial wastewater contains other chemicals in addition to dye [3]. The treatment methods for dye effluent can be divided into three categories, namely physical treatment, biological treatment and chemical treatment. Recently, photoinduced catalytic degradation technology has attracted a lot of attention to solve this challenging problem [4]. A variety of nanomaterials can be applied for photocatalysis wastewater treatment, especially titanium oxide (TiO_2), is considered as an excellent photocatalyst in this class due to its lower cost, high stability in a broad pH range, higher efficiency, low toxicity, easy availability, environmentally friendly, and highly oxidizing photogenerated holes [5]. Since the components of composite have some synergistic effects to limit the main drawback of photocatalysis systems such as rapid recombination of electrons (e^-) and holes (h^+) and visible light activation, it is believed that composite of co-photocatalysts will partially satisfy the difficult acquisition [6,7]. However, a wider variety of methods are described in papers to give a more comprehensive understanding of the nanophotocatalysts with high efficiency utilized such as doping with metal nanoparticles and then photocatalysts-

Corresponding Authors: Mahmoud Salimi
ma.salimi@iau.ac.ir

based nanocomposite fabrication [8-10]. The main objective of this research work is to prepare high performance, low cost combined nanophotocatalyst composite with synergistic effect with prospective benefits for future industrial application solutions. A series of TiO_2/SBA-15 photocatalysts with different Si/Ti ratios were synthesized by Akbay and Göl using a one-step hydrothermal method with TiO_2 nanopowder as the titanium source [11]. The photocatalytic activities of TiO_2/SBA-15 nanophotocatalysts were evaluated by photodegradation of methylene blue under UV light irradiation at constant TiO_2 content. The highest efficiency was obtained in the TiO_2/SBA-15 (Si/Ti = 16) photocatalyst at 79.6%, which is higher than the activity of bulk TiO_2 photocatalyst. Their results show that the photocatalyst activity and stability are good. The photocatalytic activity was sustainable after reuse for several cycles.

Here, it was used by a one-step microwave-assisted hydrothermal method for preparing Ag-TiO_2/SBA-15 nanophotocatalyst. The prepared photocatalysts were characterized by types of different analytical methods, XRD, SEM-EDX, UV-DRS, and N2 adsorption-desorption isotherms. The effect of the Ag/TiO_2 ratio on the photocatalytic activity in the degradation of MO under the irradiation of visible light has been investigated. In addition, six runs were carried out to test the reusability and stability of Ag-TiO_2/SBA-15 photocatalysts.

2. Experimental

2.1. Materials

Tetraethyl orthosilicate (TEOS) as silica source, Pluronic-123 copolymer (triblock poly(ethylene oxide)-poly(propylene oxide)-poly(ethylene oxide) were purchased from Sigma Aldrich. HCl (37%) was purchased from Merck. Titan(IV)-oxid nanopowder, 21 nm primary particle size (TEM), ≥99.5% trace metals basis, (35-65 m^2/g , BET) and its molecular weight was 79.90 g/mol. $AgNO_3$ as source of silver nanoparticles, dimethylaminoazobenzene-4-sulfonic acid, sodium salt as methyl orange (MO) dye ($C_{14}H_{14}N_3NaO_3S$) as a pollutant model was purchased from Merck, and its molecular weight was 327.34 g/mol with absorption peak at 507 nm in water + 0.5 ml 1N hydrochloric acid.

2.2. Preparation of Ag-TiO_2/SBA-15 nanophotocatalyst

The procedure involved mixing 4 g Pluronic-123 with 30 ml distilled water in a magnetic stirrer at 35°C for 3 hours and then adding 150 ml 2M HCl [11]. In this step, a series of desired amounts of $AgNO_3$ and a fixed amount of TiO_2 nanopowder were added and stirred for 3 hours. Different Ag/TiO_2 ratios were formed. Then, a cloudy solution consisting of Ag ions dispersed on the surface of TiO_2 was placed in domestic microwave (Samsung Solo Microwave, 1000W: MS32DG4504ATE3) for 10 minutes to form Ag nanoparticles. The color of the Ag nanoparticles changed to dark brown [12,13]. TEOS of 12 ml was then added to the above solutions and the resulting systems were kept at room temperature for 20 min. The mixtures were stirred for 20 h at 40 °C and allowed to react overnight at 100 °C in Teflon containers. The solid product was filtered and washed with deionized water. Excess HCl was extracted. Drying was carried out at 30 °C for 45 hours and calcination was carried out at 600 °C (30 °C/min) under an air flow for 5.5 h.

2.3. Characterization

To confirm the phase of titania and Ag nanoparticles, X-ray diffraction (XRD) analysis was performed using an X-ray diffractometer (Philips) and Cu-Kα (1.54 Aº) radiation with the scanning range from 2Θ=80° to 2Θ=1o° at a rate of 2° min^{-1}. The BET (Brunauer-Emmett-Taller) specific surface area was obtained from N_2 adsorption-desorption isotherm measured at 77 K in an automated adsorption apparatus (Tristar II 3020 Operator's Manual v3.02, Micrometric). To obtain information about the surface morphology of the catalysts, images were taken at different magnifications on the HITACHI TM 3030 Plus brand SEM. A UV-Vis spectrophotometer (Shimadzu UV-3600) was used for UV diffuse reflectance spectra (DRS) in the range of 200 to 500 nm to approve the visible light active nanophotocatalyst preparation. UV-Vis technique (Perkin Elmer Lambda 25 UV-Vis Spectrophotometer) was used to determine Ag nanoparticles formation on the surface of TiO_2 and also surface plasmon resonance for all samples with different Ag/TiO_2 ration.

2.4. Photocatalytic study

The photocatalytic activities of the synthesized nanophotocatalysts were investigated by photodegrading MO dye under visible light irradiation. A glass beaker as reactor system with temperature control was used for

photocatalytic experiments. A tungsten halogen lamp (250 W) was used as the light source. In a typical run, 50 ml of MO at 12 ppm concentration was prepared and then a known amount of catalyst (3 mg) was added to the solution. To obtain the adsorption-desorption equilibrium, the reaction mixture was magnetically stirred in the dark for 15 min before exposure to visible light. By taking 2 ml of the reaction mixture, the catalyst was removed by centrifugation at 13000 rpm for 20 min. at given time intervals of 15 min. The concentration of the samples was determined using the UV-Vis spectrophotometer (SHIMADZU UV-2600 UV Spectrophotometer device). The photodegradation of the MO solution was followed by the decrease in intensity of the absorption band of the MO spectra, typically at 507 nm. The degradation efficiency of the MO was calculated by using the following Eq. (1):

$$\text{MO photodegradation (\%)} = \left(1-\frac{A_t}{A_0}\right) \times \mathbf{100} \quad (1)$$

3. Results and discussion

3.1. UV-Vis analysis

UV-Vis analysis of synthesized Ag-TiO_2/SBA-15 photocatalysts with different Ag/TiO_2 ratios were performed and given in Fig. 1. It was observed that all samples have an absorption band at wavelengths from 400 to 450 nm. The SPR of nanocomposite photocatalysts are slightly redshifted with increasing Ag/TiO_2 ratios, indicating that the Ag nanoparticles agglomerate on the surface of TiO_2 nanoparticles.

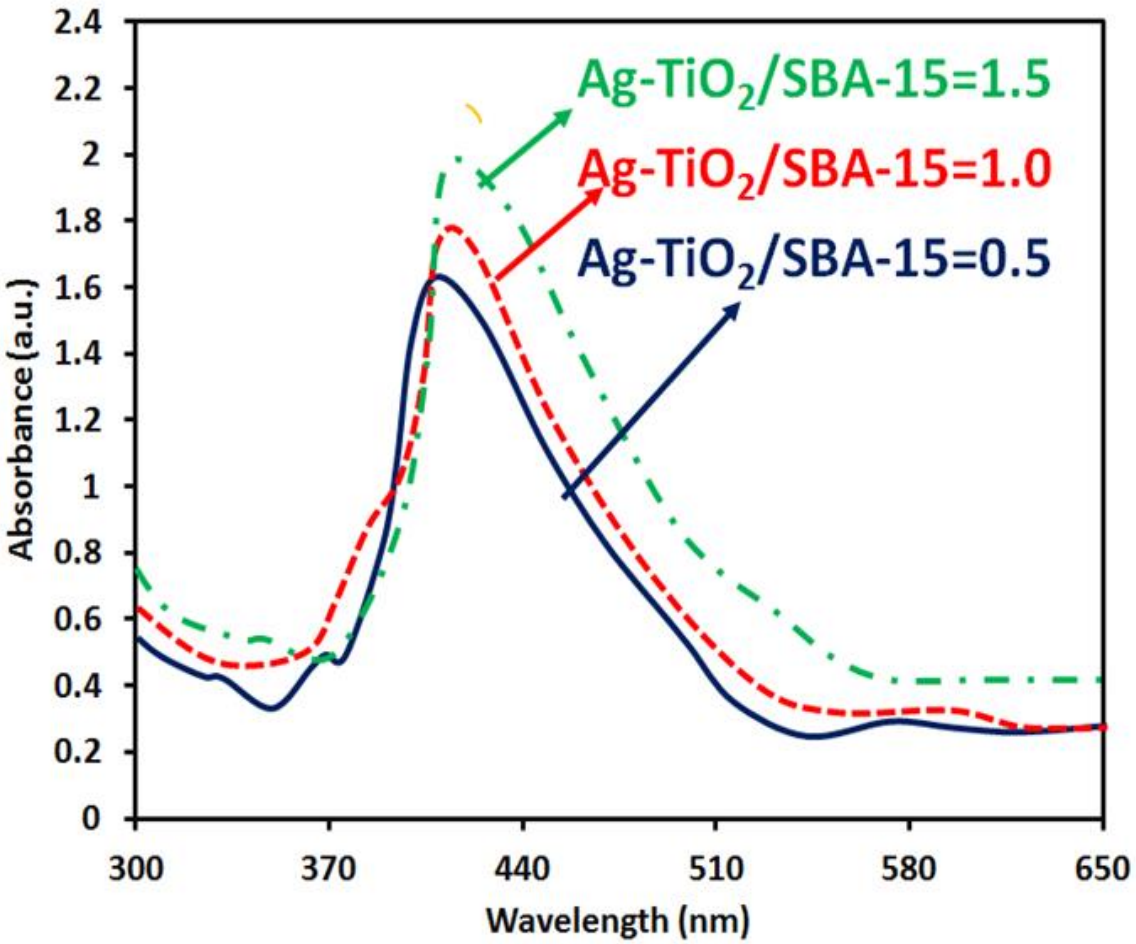

Fig. 1. UV-Vis analysis of synthesized Ag-TiO_2/SBA-15 photocatalysts with different Ag/TiO_2 ratios

3.2. XRD study

The wide-angle X-ray diffraction patterns of the synthesized catalysts have confirmed the presence of any crystalline species in the mesoporous Ag-TiO_2/SBA-15(Ag/TiO_2:1.0) nanophotocatalyst (Fig. 2). As shown in Fig. 1b, the Ag-TiO_2/SBA-15 (Ag/TiO_2:1.0) nanophotocatalysts have a pattern with a broad peak centered at 2θ ≅ 23°, corresponding to the amorphous silica walls of SBA-15. The new diffraction peaks appearing at ≅ 25° (101), 38° (004), 48° (200), 54° (105), 55° (211), and 63° (204) show the crystal structure of anatase TiO2. No diffraction peaks were detected corresponding to the rutile TiO2 phase, whereas the pure TiO2 shows both anatase (JCPDS card no. 01-084-1285) and rutile phases (JCPDS card no. 01-088-1172) [12].

This indicates that the rutile phase was completely transformed into the anatase phase during the synthesis of the photocatalyst. The results showed that the Ag nanoparticles formed a semi-cubic crystal structure with diffraction angles of 38.52, 44.39, 64.89, and 77.68. These angles correspond to the crystal faces of the Braggs reflection patterns at 2θ, and these patterns correspond to (111), (200), (220) and (311). The diffraction peaks were compared with the standard data (JCPDS file No. 04-0783), which showed that the face-centered cubic (FCC) of the silver nanoparticle was successfully prepared [13].

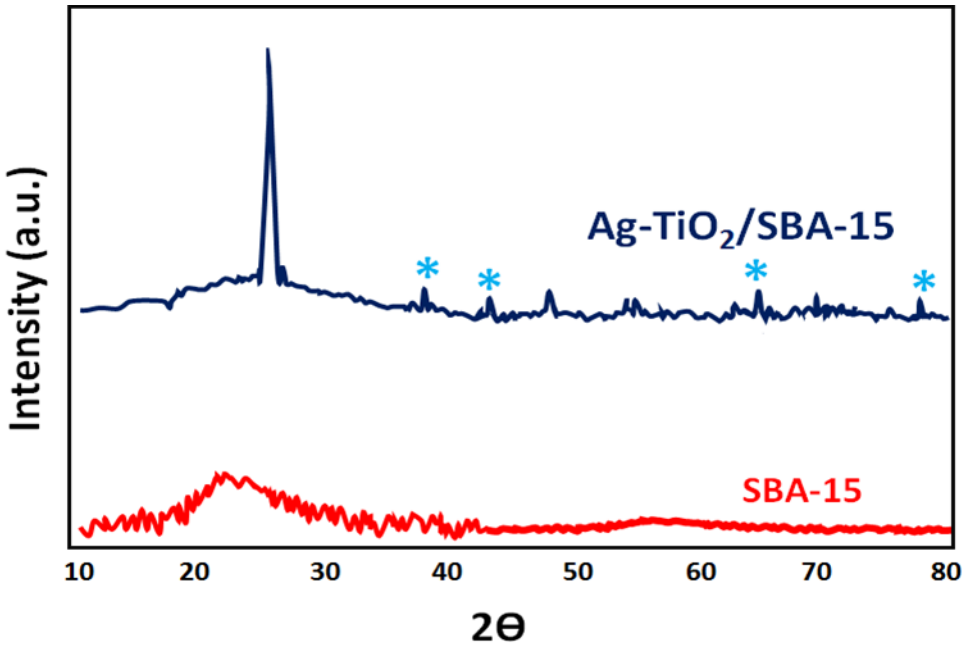

Fig. 2. The wide-angle X-ray diffraction patterns of the synthesized Ag-TiO_2/SBA-15(Ag/TiO_2:1.0) nanophotocatalyst and SBA-15.

3.3. BET

The N_2 adsorption-desorption isotherm method was used to investigate the textural properties of SBA-15 and Ag-TiO_2/SBA-15(1.0) samples. The N_2 adsorption-desorption isotherms and the pore size distribution curves of the synthesized SBA-15 and TiO_2/SBA-15(1.0) are shown in Fig. 3. The synthesized SBA-15 and Ag-TiO_2/SBA-15(1.0) exhibited type IV characteristic curves with type H1 hysteresis loop, according to the IUPAC classification [14]. The SBA-15 exhibited the hysteresis loop at high relative pressures ($0.6 < p/p_0 < 0.8$) in a range that represents the self-filling of mesopores due to capillary condensation, indicating the presence of uniform mesopores. The synthesized Ag-TiO_2/SBA-15(1.0) photocatalysts (showed a hysteresis loop with a little bit low relative pressure ranges ($0.5 < p/p_0 < 0.8$) due to the reduction of the mesopore size with some of the small Ag-TiO_2 particles dispersed in the pores of SBA-15.

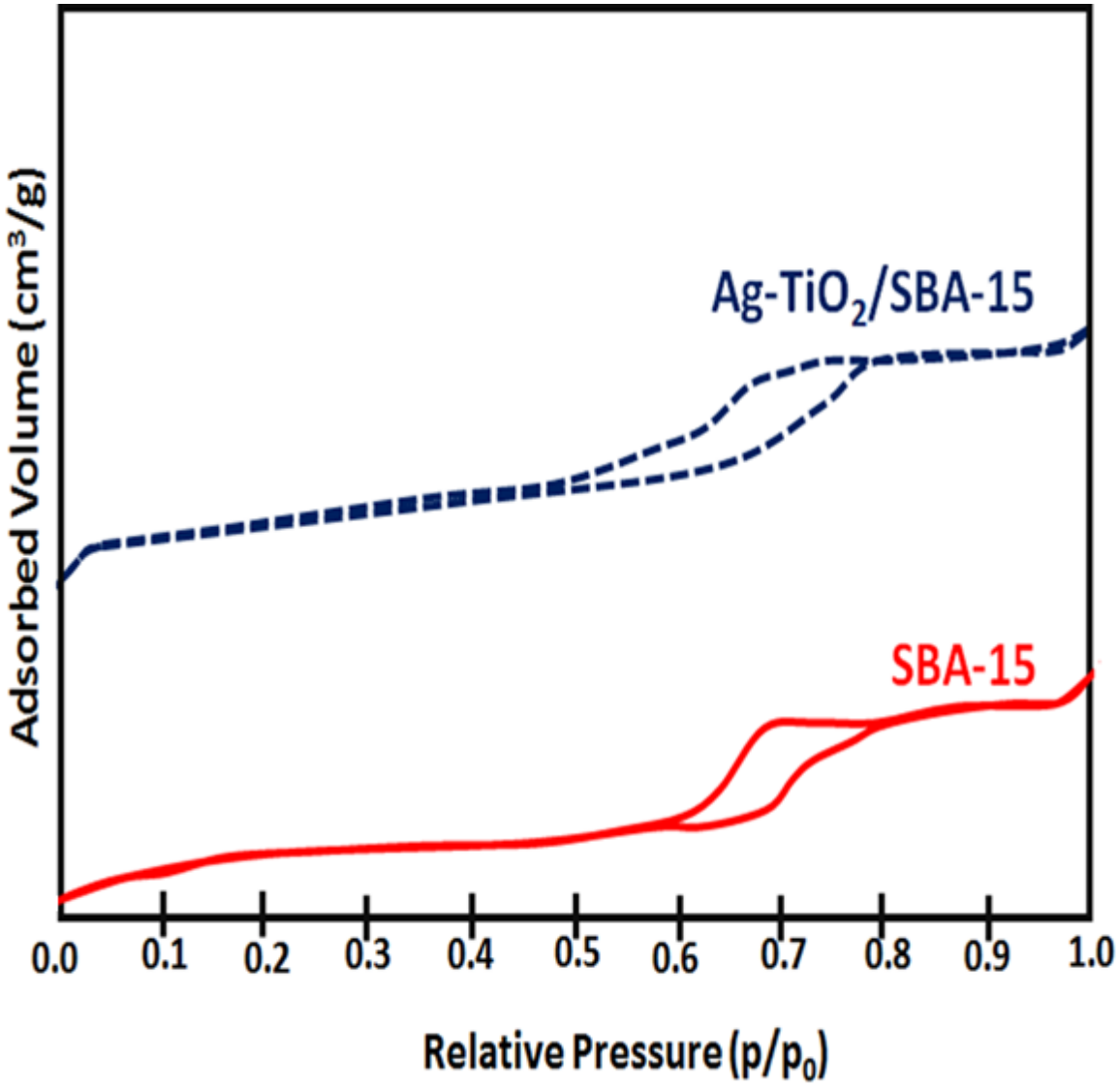

Fig. 3. The N_2 adsorption-desorption isotherm to investigate the textural properties of SBA-15 and Ag-TiO_2/SBA-15(1.0) samples.

3.4. DRS

DRS analysis of synthesized Ag-TiO_2/SBA-15(1.0) photocatalyst was performed and shown in Fig. 4. Diffuse reflectance spectroscopy is a scientific technique used to probe the optical band gap energy of nanomaterials. The Kubelka-Munk function along with the Tauc plot method can be used to determine the optical band gap energy of Titanium Dioxide. Band gap indicates the difference in energy between the top of the valence band filled with electrons and the bottom of the conduction band devoid of electrons. It was observed that nanophotocatalyst sample have an absorption band at wavelengths from 250 to 450 nm, and the wavelength of cut-off absorption around 430 nm, which is confirmed the sensitization of TiO_2 with low band gap compared to the absorb on the bandgap of anatase TiO_2. Quantization effects that improve the photocatalytic properties are indicated by the increase in band gap energy of Ag-TiO_2/SBA-15.

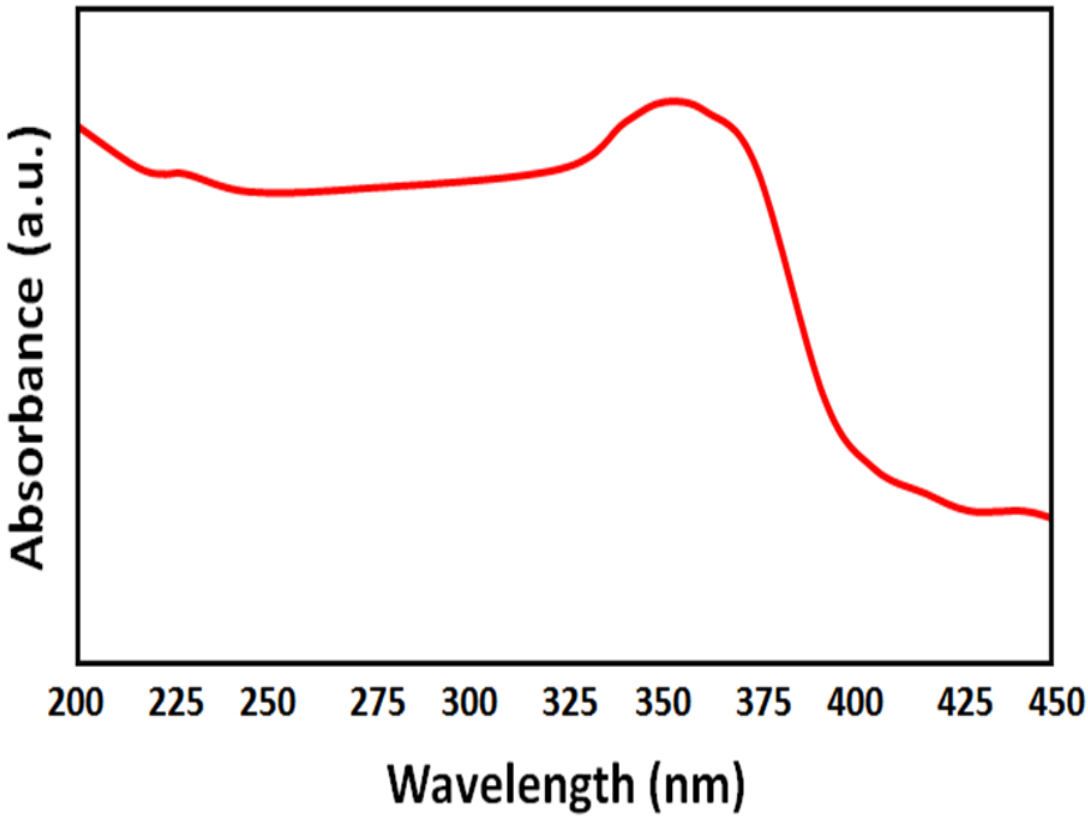

Fig. 4. DRS analysis of synthesized Ag-TiO_2/SBA-15(1.0) photocatalyst

3.5. AFM

The AFM images of the synthesized SBA-15 and different Ag-TiO_2/SBA-15(Ag/TiO_2: 0.5, 1.0 and 1.5) are given in Fig. 5(a-d). Atomic force microscopy analysis provides images with near-atomic resolution for measuring surface topography. A typical AFM can create 3D topography images with a range over hundreds of microns at subnanometer resolution. The out-of-plane resolution of AFM can reliable resolve single atomic layer steps of graphene, which is around 0.35 nm. AFM is also referred to as Scanning probe microscopy. Atomic Force Microscopy is capable of quantifying surface roughness of samples down to the angstrom-scale. As can be seen in Fig. 4-a, the SBA-15 has agglomerated tubular-like morphology. SEM images of Ag-TiO_2/SBA-15(0.5) catalyst given in Fig. 2b-e. SBA-15 retained the filamentous structure to prevent the collapse of the silica mesostructure after Ag-TiO_2 nanoparticles were inserted into the silica framework. It was observed that Ag-TiO_2 nanoparticles were distributed evenly on the SBA-15 pore walls in Ag-TiO_2/SBA-15 photocatalysts by Ag-TiO_2 nanoparticles at ratio of 1.0. The underlying principle of AFM is that this nanoscale tip is attached to a small cantilever which forms a spring. As the tip contacts the surface, the cantilever bends, and the bending is detected using a laser diode and a split photodetector. This bending is indicative of the tip-sample interaction force. Fortunately, the AFM technique has evolved rapidly to realize new capabilities and overcome existing limitations based on experimental needs by proper modification of the AFM system and combination with other techniques. Fig. 5-d displays that the SBA-15 pores are slightly clogged by Ag-TiO_2 nanoparticles at high ratio of 1.5 with agglomeration of Ag-TiO_2 nanoparticles.

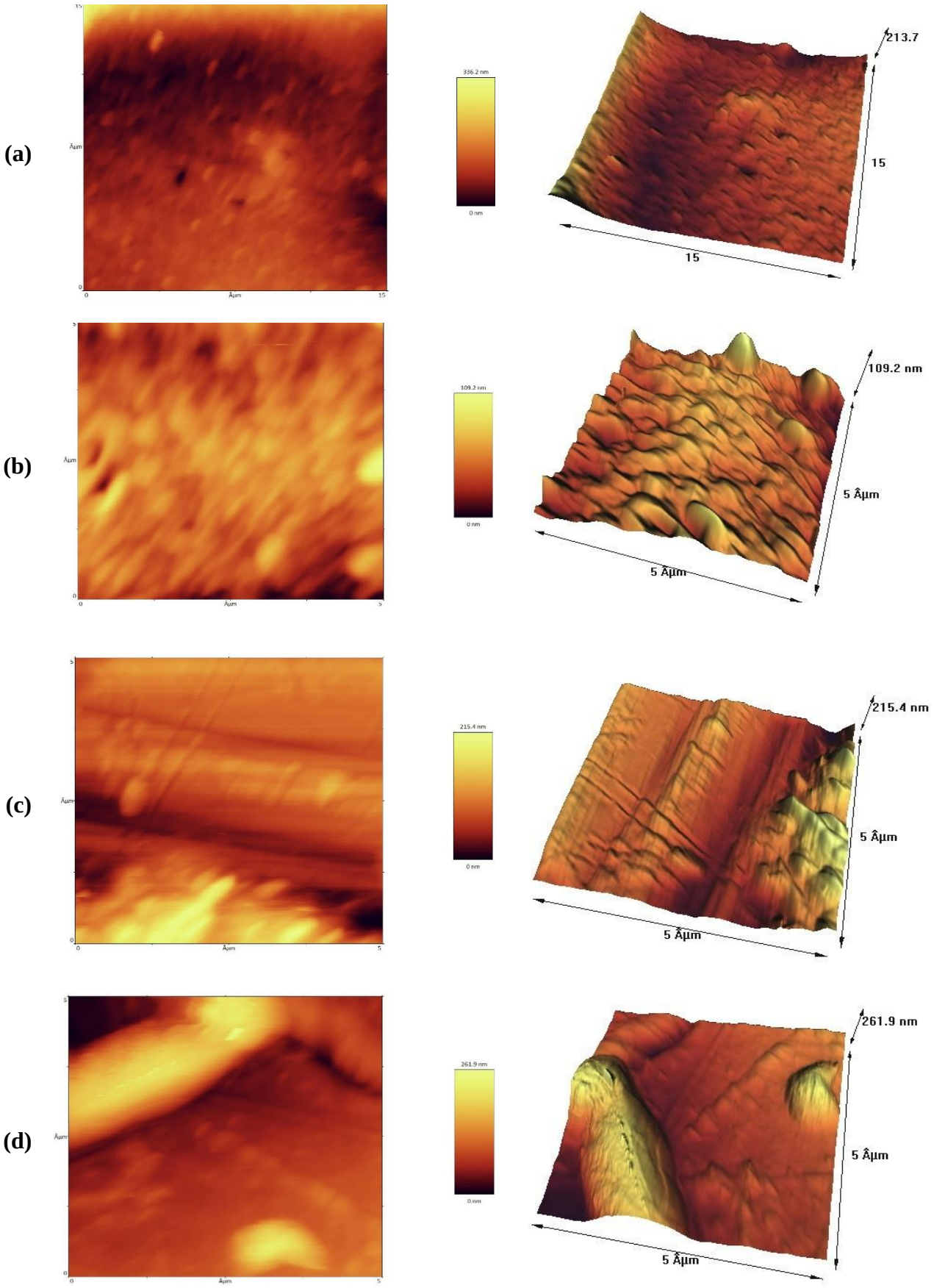

Fig. 4. The AFM images of the (a) SBA-15, Ag-TiO_2/SBA-15 (b) 0.5, (c) 1.0, and (d) 1.5 ratio of Ag/TiO_2, (5µ×5µ) space was used to scan.

3.6. Photocatalytic investigation

3.6.1. The effect of the Ag/TiO_2 ratio

Results of photocatalyst efficiencies of Ag-TiO_2/SBA-15 photocatalysts with different Ag/TiO_2 ratio are given in Fig. 5. Photocatalytic activities of Ag-TiO_2/SBA-15 with different Ag/TiO_2 ratio to evaluate the effect of Ag/TiO_2 by photodecoloration of MO under visible light illumination were tested and all result are shown in Fig. 6.As a comparative study and confirmation the role of Ag/TiO_2 ratio due to quantization effect and also the advantage of dispersion/inserted of Ag/TiO_2 on the surface of SBA-15, their photocatalytic efficiencies, were investigated in contrast of the three col samples including MO self-photolysis, SBA-15 and TiO_2 nanopowder. The amount of all samples and conditions were constant and same, which is 6 mg of samples was employed. As seen in Fig. 5, the first blank tests as MO self-photocatalysis was made out in the absence of a nanophotocatalyst and no MO photodegradation was observed. The second control test was carried in the presence of SBA-15, and same to the first control sample test, the concentration of MO, no changed after the visible light illumination was turned on, indicating the SBA-15 reached the adsorption equilibrium of MO (Fig. 5).

It is clear that the SBA-15 mesoporous sample has no photocatalytic activity due to no radical groups composed of reactive oxygen species (ROS) formation in an amorphous silica structure. TiO_2 nanopowder have low photocatalytic activity in UV region due to high band-gap energy of TiO_2 and low UV part of applied lamp in this test. Anothe reseon is the poor dispersion of active phases. Its photocatalytic efficiency is increased as a result of high dispersion of TiO_2 into the SBA-15 in all synthesized photocatalyst. This result shows that the titanium incorporated into SBA-15 framework is enhanced the photoactivity of TiO_2. As seen in Fig. 5, MO degradation was increased, with increasing Ag/TiO_2 ratio to 1.0. So, among them, Ag-TiO_2/SBA-15 (Ag/TiO_2:1.0) presented the best MO photodegradation performance.

Therefore, the improved photocatalytic activity should be attributed to the insert of the Ag-TiO_2 particles in the SBA-15 pore walls. Also, this phenomenon is seen in the pore distribution images of AFM analysis. These results show that good Ag-TiO_2 dispersion into the SBA-15 reveals more active sites near the adsorbed dye molecules, resulting in an increase in degradation rates.

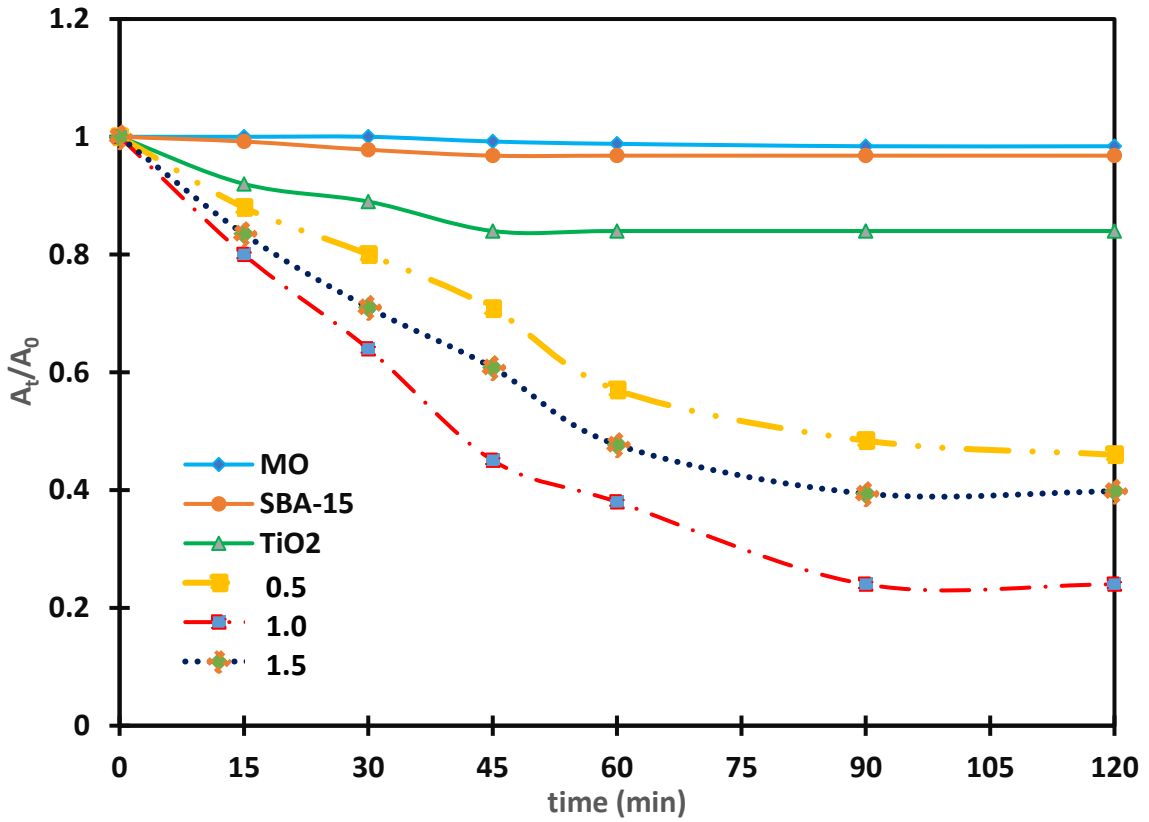

Fig. 5. Photocatalyst efficiencies of Ag-TiO_2/SBA-15 photocatalysts with different Ag/TiO_2 ratio compared to the MO self-photolysis, SBA-15 and TiO_2 nanopowder.

3.6.2. The effect of pH

Results of photocatalyst efficiencies at different pH over Ag-TiO_2/SBA-15 (1.0) nanophotocatalysts are presented in Fig. 6. The amount of nanophotocatalyst for each pH test were constant and same, which is 6 mg of sample nanophotocatalyst was employed. As seen in Fig. 6. it is obvious that in the pH=4 photocatalytic efficiency is increased. Thus, the best pH value for MO photodegradation is obtained at 4. As can be seen from these results, either increasing or decreasing the pH value from 4, the photocatalytic efficiencies will decrease significantly. In fact, the change in pH plays a critical role in the adsorption of dye molecules on the surface of the photocatalyst and then the photodegradation reaction. In other words, changing the pH can change the surface charge of the photocatalyst or change the charge of the dye molecules and then affect the interaction between the dye molecules and the nanocomposite surface [15]. Photodegradation of anionic MO dye, which has negatively charged groups due to the presence of sulphuric group in its structure, better attraction of MO molecules to the Ag-TiO_2/SBA-15 nanocomposite surface will occur at pH = 4.

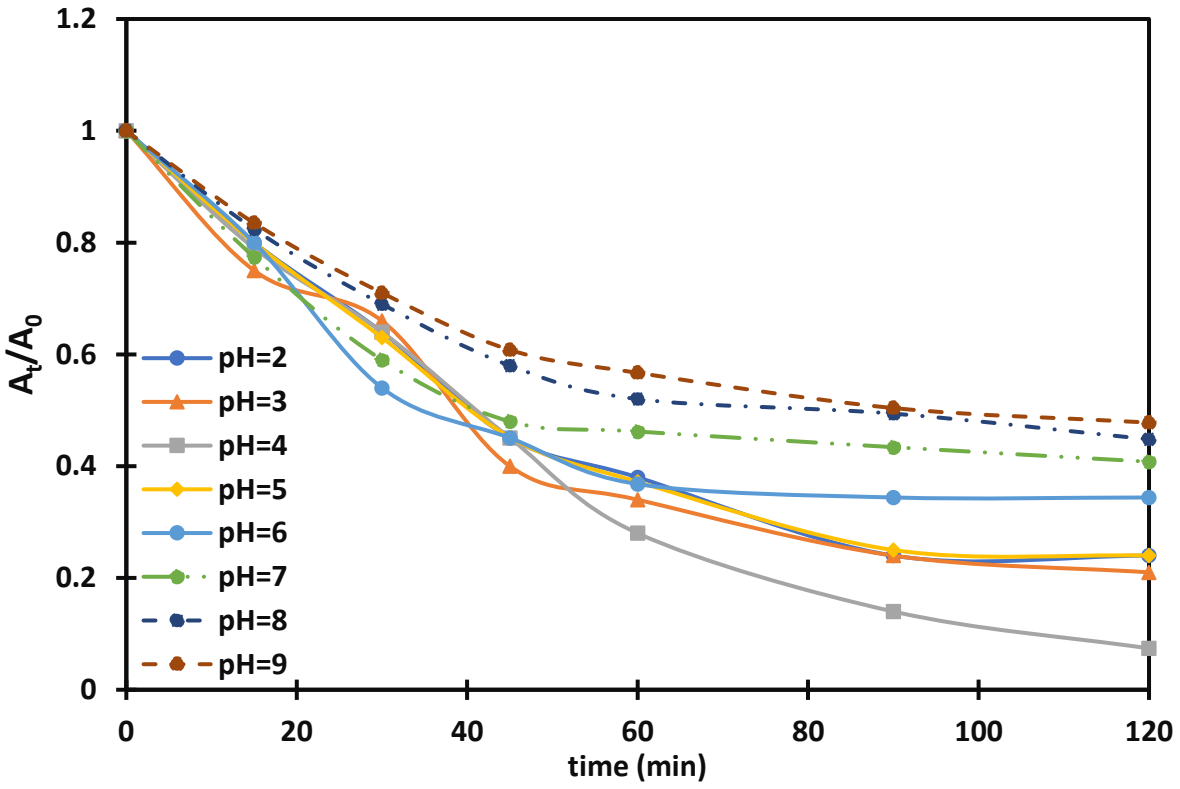

Fig. 6. The effect of pH on the photocatalytic activity of Ag-TiO_2/SBA-15 (1.0) nanophotocatalyst for MO photodegradation

3.6.3. Reusability and stability study

Photocatalyst stability and reusability as one of the major factors in the heterogeneous photodegradation industries were conducted on the Ag-TiO_2/SBA-15 (1.0) nanophotocatalyst and optimum pH for six runs and are given in Fig. 7. Each of run was studied by using the fresh MO dye solution in the presence of the same amount of the used Ag-TiO_2/SBA-15 (1.0) nanophotocatalyst. As can be8seen in Fig. 7, the activity of the reused catalyst in the 6^{th} run was the same as that of the fresh catalyst and no remarkable changes was observe. Therefore, the prepared nanophotocatalyst could use for long periods without loss of activity.

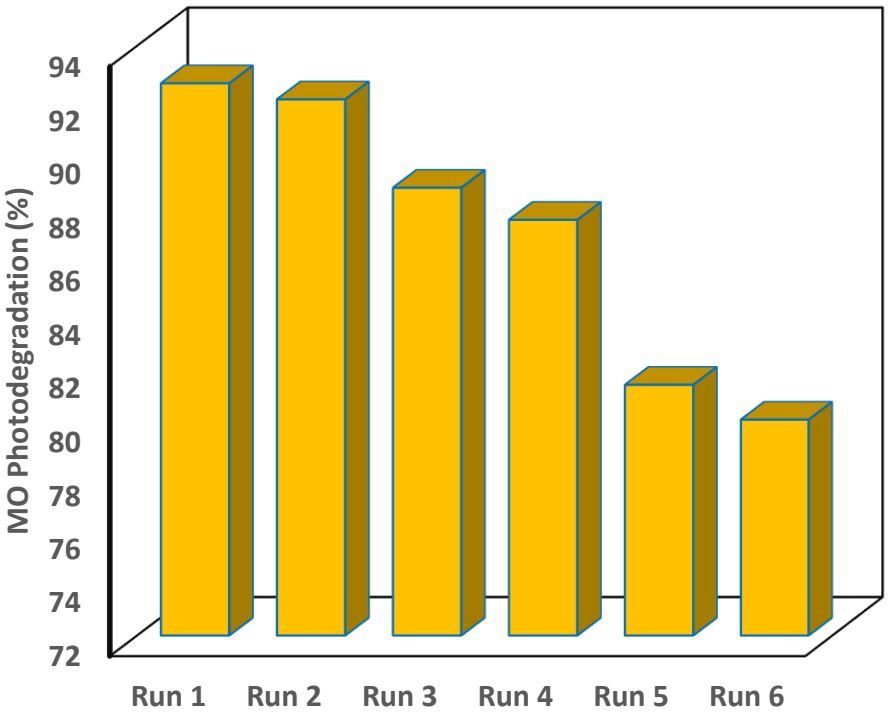

Fig. 7. Photocatalyst stability and reusability of the Ag-TiO_2/SBA-15 (1.0) nanophotocatalyst at optimum pH for six runs

4. Conclusion

A one-step microwave-assisted hydrothermal method for the preparation of Ag-TiO_2/SBA-15 nanophotocatalyst is presented in this work. XRD, N_2 adsorption-desorption isotherms-desorption isotherms, AFM, UV-Vis and UV-DRS analyses were carried out for the characterization of the obtained photocatalyst samples. At high Ag loading on the surface of TiO_2 nanoparticles, agglomeration of silver nanoparticles and also clogging in the SBA-15 pores occurs and is confirmed by AFM analysis. The optical band gap energies obtained by DRS analysis were significantly blue-shifted, which is the quantization effect that improves the photocatalytic activities under visible light illumination due to the presence of silver nanoparticles that act as photosensitizer and reduce the recombination of the formed charge carriers (e and hole). The photocatalytic performances of the Ag-TiO_2/SBA-15 nanophotocatalyst were evaluated by the photodegradation of methyl orange (MO) dye at different Ag/TiO_2 ratios. In MO destruction experiments, the highest photocatalytic efficiency was obtained in the Ag/TiO_2-SBA-15 (Ag:TiO_2=1.0) photocatalyst at 76.0%, and all the efficiencies over the synthesized nanophotocatalyst are higher than commercial bulk TiO_2 nanophotocatalyst activity due to the low UV part of the applied visible light halogen lamp and also Ag/TiO_2 nanophotocatalyst, which may be due to the poor dispersion of active phases. Ag-TiO_2/SBA-15 (1.0) at pH=4 showed the highest photocatalytic efficiency. The photocatalyst can be reused six times without losing its efficiency. This shows that the photocatalyst is stable and can be used over and over again.

Conflicts of Interest

The author declares no conflict of interest.

Author information

*Corresponding Author: Mahmoud Salimi
E-mail address: ma.salimi@iau.ac.ir

References

[1] S. Rafaqat, N. Ali, C. Torres, B. Rittmann, Recent progress in treatment of dyes wastewater using microbial-electro-Fenton technology. RSC Adv. 12(27) (2022) 17104-17137 https://doi.org/10.1039/d2ra01831d.

[2] B. Lellis, C.Z. Fávaro-Polonio, J.A. Pamphile, J.C. Polonio, Effects of textile dyes on health and the environment and bioremediation potential of living organisms. Biotechnol. Res. Int., 3(2) (2019)275–290. https://doi.org/10.1016/j.biori.2019.09.001

[3] Y. Feng, X. Su, Y. Chen, Y. Liu, X. Zhao, C. Lu, Y. Ma, G. Lu, M. Ma, Research progress of graphene oxide-based magnetic composites in adsorption and photocatalytic degradation of pollutants. A review Mater Res Bull.162 (2023) 112207. https://doi.org/10.1016/J.MATERRESBULL.2023.112207.

[4] H. Wu, H.L. Tan, C.Y. Toe, J. Scott, L. Wang, R. Amal, Y.H. Ng YH, Photocatalytic and photoelectrochemical systems: Similarities and differences. Adv. Mater., 232 (2020) 1–21. https://doi.org/10.1002/adma.201904717.

[5] N.C. Joshi, P. Gururani, S.P. Gairola, Metal oxide nanoparticles and their nanocomposite-based materials as photocatalysts in the degradation of dyes. Biointerface Res. Appl. Chem. 12 (2022) 6557–6579. https://doi.org/10.33263/BRIAC125.65576579.

[6] R. Shanmuganathan, F. Lewis Oscar, S. Shanmugam, N. Thajuddin, S.A. Alharbi, N.S. Alharbi, K. Brindhadevi, A. Pugazhendhi, Core/shell nanoparticles: Synthesis, investigation of antimicrobial potential and photocatalytic degradation of Rhodamine B. Journal Photochem. Photobiol. B Biol. 202 (2020) 111729. https://doi.org/10.1016/j.jphotobiol.2019.111729.

[7] K. Shaheen, H. Suo, T. Arshad, Z. Shah, S.A. Khan, S.B. Khan, M.N. Khan, M. Liu, L. Ma, J. Cui, Y.T. Ji, Y. Wang, Metal oxides nanomaterials for the photocatalytic mineralization of toxic water wastes under solar light illumination. J. Water Processing Eng. 2020;34:101138. https://doi.org/10.1016/J.JWPE.2020.101138.

[8] A. Salabat, F. Mirhoseini, F.H. Nouri, Microemulsion strategy for preparation of TiO_2–Ag/poly(methyl methacrylate) nanocomposite and its photodegradation application. J. Iranian Chem. Soc. 20 (2022) 599–608. https://doi.org/10.1007/s13738-022-02693-7.

[9] A. Salabat, B.S. Mirhoseini, F. Mirhoseini, Ionic liquid based surfactant-free microemulsion as a new protocol for preparation of visible light active poly(methyl methacrylate)/TiO_2 nanocomposite. Sci Rep 14, 15676 (2024). https://doi.org/10.1038/s41598-024-66872-7

[10] A. Salabat, F. Mirhoseini, Applications of a new type of poly(methyl methacrylate)/TiO_2 nanocomposite as an antibacterial agent and a reducing photocatalyst. Photochem. Photobiol. Sci., 14(9) (2015) 1637–1643. https://doi.org/10.1039/c5pp00065c

[11] S.C. Göl, E. Akbay, Reusable titania-SBA-15 photocatalyst synthesized by different silica/titania ratios for enhancing methylene blue photodegradation. *In Research Square*. https://doi.org/10.21203/rs.3.rs-1831676/v1

[12] L.A. Calzada, R. Castellanos, L.A. García, T.E. Klimova, TiO_2, SnO_2 and ZnO catalysts supported on mesoporous SBA-15 versus unsupported nanopowders in photocatalytic degradation of methylene blue. Microporous Mesoporous Mater 285 (2019) 247–258. https://doi.org/https://doi.org/10.1016/j.micromeso.2019.05.015

[13] S. Mayachar, N. Nandini, A.J. Adur, Optimization, characterization and antibacterial activity of green synthesized silver nanopaticles using Moringa oleifera leaf extract. Research J. Chmical Environ. Sci., 5(6) (2018) 48–57.

[14] T. Qiang, Y. Song, J. Zhao, J. Li, Controlled incorporation homogeneous Ti-doped SBA-15 for improving methylene blue adsorption capacity. J. Alloys Compd., 770 (2019) 792–802. https://doi.org/https://doi.org/10.1016/j.jallcom.2018.08.074

[15] F. Mirhoseini, A. Salabat, Ionic liquid based microemulsion method for fabrication of poly(methyl methacrylate)–TiO_2 nanocomposite as highly efficient visible light photocatalyst, RSC Adv. 5 (2015) 12536–12545. https://doi.org/10.1039/c4ra14612c